Original Research Paper

Characterization of Activated Carbon from Eggshell Membranes Prepared Using Sodium Acetate and Zinc Metal Activation

Sumrit Mopoung and Kanjana Jitchaijaroenkul

Department of Chemistry, Faculty of Science, Naresuan University, Phitsanulok 65000, Thailand

Abstract: The eggshell membranes of ducks and hens were carbonized or activated with 4 wt% sodium acetate or zinc at 400-600°C. The carbonized or activated products were characterized by SEM-EDS, TEM, FTIR and XRD. It was found that the suitable activation temperature for eggshell membranes is 500°C with 30.03-35.26% yield. The activation performance of CH_3COONa for eggshell membrane activated carbon production was higher than that of Zn metal. The CO_3^{2-}, Ca-O, C=C, Na-O and C-O functional groups have been formed on the surface of eggshell membrane activated carbon materials during both CH_3COONa and Zn activation. Furthermore, CaO, MgO, Na_2O and ZnO have also accumulated on eggshell membrane activated carbon materials with high content and regular dispersion. It was shown that the particles on the duck eggshell membrane activated carbon formed with Zn had weaker attachment on the surface than for duck eggshell membrane activated carbon formed with CH_3COONa at same temperature. The XRD and TEM results revealed that the eggshell membrane activated carbons consist of an amorphous carbon matrix with some disordered graphite carbon matrix, spherical particles and nanofiber.

Keywords: Eggshell Membrane, Activated Carbon, Sodium Acetate, Zinc

Introduction

Large quantities of egg waste are discarded worldwide. They consist of egg shells and Eggshell Membranes (ESM) (Mittal *et al*., 2016). The ESM resides between the egg white and the inner surface of the eggshell (Tsai *et al*., 2006). The Hen Eggshell Membrane (HESM) consists of interwoven protein fibers and spherical masses (Tsai *et al*., 2008). The duck egg contains about 11% eggshell and ESM. It also consists of an inner and an outer membrane with entangled threads or randomly knitted net shapes. The diameter of ESM fiber is less than 0.2 μm (Kaewmanee *et al*., 2009). Furthermore, ESM also consists of yolk spherocrystal with diameter of about 30 μm (Tong *et al*., 2008). The ESM possess a porous and fibril structure, with a very high surface area and special functional groups such as hydroxyl (-OH), thiol (-SH), carboxyl (-COOH), amino (-NH₂), amide (-CONH₂) etc., which strongly interact with various chemical species (Mittal *et al*., 2016). The protein fibers of ESM are arranged to form a semi-permeable membrane which possesses an intricate lattice

of hierarchically ordered macroporous network of stable and water-insoluble fibers, which also has high surface area (Tsai *et al*., 2006). It has a high decomposition temperature (>220 °C), enough mechanical strength and low water uptake and swelling properties (<10%) (Yu *et al*., 2012) resulting its use in various applications such as adsorbents (Tsai *et al*., 2006). The ESM has also been used for adsorption of chlorinated phenols, Direct Red 80 and Acid Blue 25, from aqueous solutions (Guru and Dash, 2014). Since ESM is a highly cross-linked protein structure with excellent permeability to substrates and products (Tembe *et al*., 2008), it has been used as the substrate and template to immobilize the layered double hydroxide formed by hydrothermal crystallization method and used as adsorbent for Cr(VI) adsorption (Guo *et al*., 2011). It has been activated by glutaraldehyde for the immobilization of the enzyme tyrosinase achieved with high effectiveness (Tembe *et al*., 2008). In general, porous carbon composites containing different metals such as Fe, Co, Pt, Ag, Ni, Sn, Mn, etc. and their species have been synthesized to be used in electrochemical, catalytic, adsorption and other

applications. Metals and metal oxides in these composites can strongly affect the structural, textural and other characteristics of the materials (Gun'ko *et al.*, 2014). For example, activated carbon from coconut shells has been modified with 10-15% sodium acetate and used in a fixed-bed column for copper ions removal. The authors have shown that the material could adsorb 33-45 mg of Cu with Cu(II): Na ratio of 3.85 mol: 7.54 mol (Mugisidi *et al.*, 2007). Zinc acetate has been used as a catalyst for polycondensation and polymer carbonization of resorcinol-formaldehyde mixtures. The mixtures were carbonized at 780-800°C to form ZnO doped chars. The texture of the doped chars depends strongly on the content of ZnO. The chars can be purely nanoporous and composed of micro sized smooth globules with low ZnO content, or composed of nano-mesoporous particles of 20-100 nm in size with high ZnO content differently aggregated into secondary meso-macroporous structures (Gun'ko *et al.*, 2014). ZnO micro/nano materials were also hydrothermally grown on activated carbon cloth and used as electrodes in a flow cell for brackish water desalination by capacitive deionization (Myint *et al.*, 2014). In addition, the nano ZnO/activated carbon composite has been used for tributyltin removal from seawater (Ayanda *et al.*, 2013).

This research studied the effect of activation agents (5wt% of sodium acetate or zinc metal) and pyrolysis temperature (400-600°C) on the preparation of carbonized and activated carbon products from duck and hen eggshell membranes. The products were characterized by FTIR, XRD, SEM-EDS and TEM. The percent yields of carbonized products and activated carbons are also calculated.

Materials and Methods

The eggshell wastes of hen and duck were obtained from local households and were washed with deionized water. The ESMs were then manually removed from outer eggshell and dried in oven (SL shellab, 1350 FX, USA) at 120°C for 3 h. The dried ESMs were mixed with 5wt% of sodium acetate (AR grade) or Zn metal powder (size 80 mesh, AR grade) by a wet method in aqueous solution. The mixtures were dried in oven at 120°C for 3 h. Accurate weights of the dried mixtures were filled into porcelain crucibles which were covered by aluminium foil followed by a lid and then activated in an electric furnace (Fisher Scientific Isotemp ® Muffle furnace) at final temperatures of 400, 500 and 600°C with a constant heating rate of 10°C min^{-1} and a 5 min soaking time. The dried ESMs were also carbonized at 400, 500 and 600°C. After reaching the final temperature and the soaking time, the final products were cooled to room temperature. The percent yields of all products were then calculated.

Characterizations

The morphological structure and elemental composition of the dried ESMs, Carbonized Eggshell Membranes (CESMs) and Eggshell Membranes Activated Carbons (ESMACs) were observed and photographed by Scanning Electron Microscopy equipped with Energy Dispersive Spectrometer (SEM-EDS, LEO 1455 VP). The CESMs and ESMACs were also characterized by X-ray powder diffract meter (PW 3040/60, X' Pert Pro MPD), FTIR (Spectrum GX, Perkin Elmer) and TEM (PHILPS, Tecnai 12).

Results and Discussion

Percent Yield

Data in Table 1 show that the percent yields of all products decrease with increase in carbonization or activation temperature. This indicates that the volatile matters such as proteins, carbohydrates and lipids (Ahmed *et al.*, 2017), in ESMs were degraded to a higher extent at higher temperatures. Furthermore, it was seen that all products from Duck Eggshell Membrane (DESM) give higher percent yields than products made from Hen Eggshell Membrane (HESM) made at the same conditions. This may be attributed to CaCO$_3$ and other metal compounds, which show higher content in DESM which than in HESM. The egg shell membranes were decomposed into CaO and other metal oxides with high content of carbonized or activated products (Table 2). Another reason may be the protein content (80-85%) of HESM (Baláž, 2014), which is higher than that of DESM. Thus, the HESM undergoes more substantial thermal degradation than DESM. Furthermore, percent yield of all products decreased at a relatively low rate from 400 to 500°C, but a higher rate from 500 to 600°C for both ESMs. This is attributed to the thermal degradation of collagen and glycan chains in the ESMs with a slow rate in the temperature range between 250 and 450°C and then with a high mass loss rate at 500-600°C (Baláž, 2014; Yu *et al.*, 2012). Additionally, it was found that the percent yields of activated products from both ESMs formed after mixing with 5wt% of CH$_3$COONa or Zn metal powder decreased more substantially than CESMs at all temperatures. This shows that both CH$_3$COONa and Zn metal result in higher rate of decomposition of ESMs by partial oxidation in comparison to the carbonization process. The percent yields of ESMACs formed in procedures using mixing with Zn metal are higher than those formed using mixing with CH$_3$COONa at same temperature. This result is attributed to poor solubilities of ZnO in the reaction mixtures (Simanjuntak *et al.*, 2011) and high thermal degradation of CH$_3$COONa.

Table 1. Percent yields of carbonized products and activated carbons from HESM and DESM with carbonization or activation temperature at 400-600°C

Types of samples	% Yield		
	400°C	500°C	600°C
CHESM	39.41	38.48	18.62
CH$_3$COONa-HESMAC	31.81	30.03	15.23
Zn- HESMAC	34.29	32.15	17.99
CDESM	42.20	41.49	23.95
CH$_3$COONa-DESMAC	33.65	31.74	19.61
Zn-DESMAC	38.89	35.26	20.10

Table 2. Elemental composition of CH$_3$COONa-DESMAC, Zn-DESMAC, CH$_3$COONa-HESMAC and Zn-HESMAC prepared at 600°C and obtained from EDS analysis

Samples	Elements composition (wt%)					
	C	O	Na	Mg	Ca	Zn
CH$_3$COONa-DESMAC	59.63	27.26	9.59	0.80	2.78	-
Zn-DESMAC	61.30	19.56	2.65	0.63	2.29	13.80
CH$_3$COONa-HESMAC	83.99	10.33	4.78	0.67	0.79	-
Zn-HESMAC	84.94	8.280	0.97	0.78	0.74	4.790

FTIR Analysis

The FTIR spectra of the Carbonized Duck Eggshell Membrane (CDESM) and Duck Eggshell Membrane Activated Carbon (DESMAC) prepared at 400, 500 and 600°C are shown in Fig. 1. Figure 1a shows that the FTIR spectrum of CDESM prepared at 400°C contains peaks at 3367 cm^{-1} (N-H bonds or C-O asymmetric stretching), 2919 cm^{-1} (C-H bonds in = C-H and = CH$_2$ groups), 1760 cm^{-1} (C=O stretching vibration in carboxylic groups), 1650 cm^{-1} (amide C=O stretching), 1431 cm^{-1} (CaO, C=C) and 712 cm^{-1} (CO_3^{2-} of calcite) (Mami et al., 2008; Baláž et al., 2016; Tan et al., 2015; Botomé et al., 2017; Zaki et al., 2006; Tsai et al., 2006). It contains features that can be attributed to amines, amides, CaCO$_3$, = C-H and =CH$_2$, which remained in CDESM after preparation at 400°C. Especially, carboxylate CO_3^{2-} of CaCO$_3$ is still not completely decomposed after preparation at 400°C, which is demonstrated by FTIR peaks at 3367, 1431 and 712 cm^{-1} of C-O asymmetric stretching and out of plane bending vibration modes (Tan et al., 2015). The peaks indicating the presence of amines and amides in the ESMs are also located at 3367 cm^{-1} with an additional peak at 1650 cm^{-1} (Tsai et al., 2006). Thus, the organic components of ESMs are not completely decomposed after the carbonization process carried out at 400°C. This result is in accord with the percent yields of CESMs at 400°C (Table 1), which are higher than those at 500-600°C. These FTIR peaks of DESM disappeared after carbonization at 500-600°C with the exception of the peak at 1431 cm^{-1}. This confirms that the functional groups on surface of the carbon material were burnt off to a large extent after the carbonization at these temperatures. This results in the decrease of the percent yield of carbonized products as well as the activated

products (Table 1). The peak at 1431 cm^{-1} is attributed to CaO (Zaki et al., 2006), as well as C=C stretching of aromatic rings (Nasrollahzadeh et al., 2016). A new peak is observed in CDESM after carbonization at 500-600 °C at 712 cm^{-1} (very weak). This peak can be attributed to calcite, which is formed by heating at 500°C and is more crystalline than the initial calcium carbonates (López Granados et al., 2007). Materials prepared with CH$_3$COONa activation (CH$_3$COONa-DESMACs, Fig. 1d-f) show FTIR spectra with peaks similar to the CDESM, but intensity of these peaks tends to be lower than for CDESM. The intensity of the peaks also decreases with increasing temperature from 400 to 600°C. Especially, the spectrum of CH$_3$COONa-DESMAC prepared at 600°C (Fig. 1f) shows peaks only at 1431 cm^{-1} (strong) and 875 cm^{-1} (very weak) which are due to CO_3^{2-} species of calcite (Zaki et al., 2006). At 400-500°C, the FTIR spectra of CH$_3$COONa-DESMACs also contain peaks at 1110 cm^{-1}, which are attributed to C-O and C-N (Baláž, 2014; Park et al., 2016). Analogously, FTIR spectra of Zn-DESMAC (Fig. 1g-i) contain peaks similar to CH$_3$COONa-DESMAC, with the exception of the spectrum of the material prepared at 400°C (Fig. 1g). The spectrum of Zn-DESMAC prepared at 400°C also contains peaks at 3367 cm^{-1}, 2919, 1700, 1600, 1431, 1350 cm^{-1} (C-OH, Kashinath et al., 2016) and 1110 cm^{-1}. These peaks also disappeared after activation at 500 and 600°C (Fig. 1h-i) where the remaining of peaks are found at 1431, 875 and 720 cm^{-1}. These peaks remaining after activation at 600°C are also attributed to CO_3^{2-} of calcite. It should be noted that calcite is usually completely decomposed into CaO above 700°C (Zaki et al., 2006). However, the peaks of C=C, Na-O and C-O stretching (Magdziarz et al., 2016) are also located at 1431 cm^{-1}, which has caused the peak at 1431 cm^{-1} to remain with high intensity for all activated

products. The FTIR spectra of CHESMs (Fig. 2a-c), CH₃COONa-HESMACs (Fig. 2d-f) and Zn-HESMACs (Fig. 2g-i) show similar trends to the FTIR spectra of corresponding DESM materials. The analysis of the FTIR spectra revealed that the CH₃COONa and Zn activations have no effect on the type of functional groups found on activated carbon products made both from DESM and HESM, but they accelerated the decomposition or modification of functional groups on surface of ESMACs. Based on the FTIR results, it can be concluded that the suitable activation temperature for the preparation of ESMs lies in the range 500-600°C, which is in line with the report of Rath *et al*. (2014).

Elements Analysis by EDS

The elemental composition of CH₃COONa-DESMAC, Zn-DESMAC, CH₃COONa-HESMAC and Zn-HESMAC prepared at 600°C, was obtained using EDS analysis. The results are shown in Table 2 and they indicate high carbon content in all of the materials. These results confirm that the ESMs have been converted into carbon during the activation process. Moreover, it can be seen that the carbon content in HESMACs for both activation reagents is higher than that of the DESMACs. This is because HESM has higher content of organic compounds than DESM, which are converted to carbon during high temperature degradation under partial oxidation conditions. Furthermore, it can be seen that CH₃COONa-DESMAC and Zn-DESMAC have higher metal content than CH₃COONa-HESMAC and Zn-HESMAC which is in line with results of percent yield reported in Table 1. The oxygen content of all

activated carbon materials is quite high, indicating high content of oxygen containing functional groups and metals oxides on surface of the activated carbon materials. Especially, oxygen content in CH₃COONa-DESMAC is very high (27.26%), which could in part originate from the CH₃COONa activating agent. Calcium shows higher content in activated carbon materials from DESM than those from HESM. These results are also in line with the FTIR results (Fig. 1 and 2). The content of Na in CH₃COONa-DESMAC and CH₃COONa-HESMAC and Zn in Zn-DESMAC and Zn-HESMAC are quite high. This is because of the CH₃COONa and Zn that were added to the ESMs for activation, which contain Na and Zn that remain in the activated products. The Mg present in the final materials originated from starting ESMs.

XRD Analysis

The XRD patterns of carbonized and activated products made from DESM and HESM display a peak at $2\theta = 25.5°$, which is assigned as the crystallographic planes of graphitic layers with disordered graphite carbon structure (Fig. 3a-f). In addition, a weak peak located at 44° is attributed to amorphous carbon (Pant *et al*., 2017). These results confirm that the organic materials originally present in the ESMs have been converted into carbon for all produced materials thus supporting the high carbon content of carbonized and activated products as shown in Table 2. Furthermore, the XRD patterns also show crystalline peaks of calcite, which remained in final products after carbonization or activation, at $2\theta = 23, 29.5, 34.2, 36, 39.5, 43.2, 48.5, 57.5, 60.5, 63, 64.5, 72$ and $81.5°$ (Slimani *et al*., 2014).
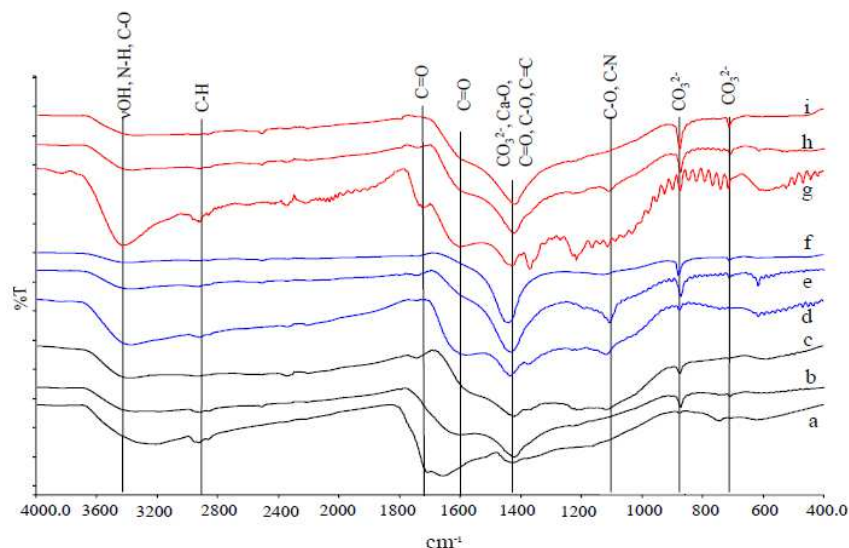

Fig. 1. FTIR transmittance spectra of (a) CDESM prepared at 400°C, (b) CDESM prepared at 500°C, (c) CDESM prepared at 600°C, (d) CH₃COONa-DESMAC prepared at 400°C, (e) CH₃COONa-DESMAC prepared at 500°C, (f) CH₃COONa- DESMAC prepared at 600°C, (g) Zn-DESMAC prepared at 400°C, (h) Zn-DESMAC prepared at 500°C and (i) Zn- DESMAC prepared at 600°C
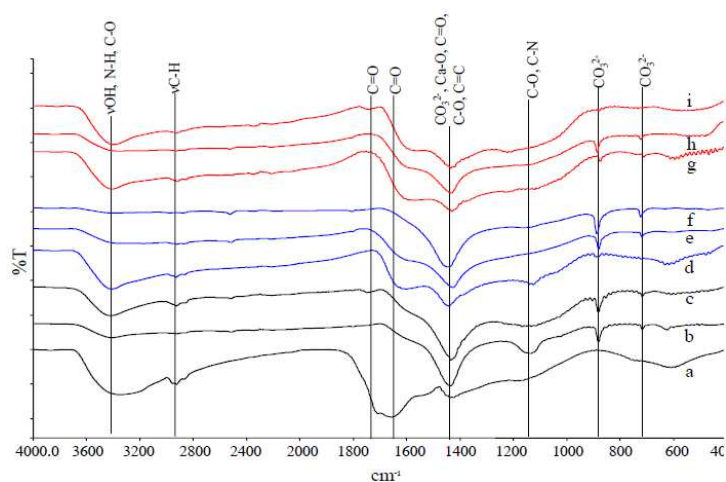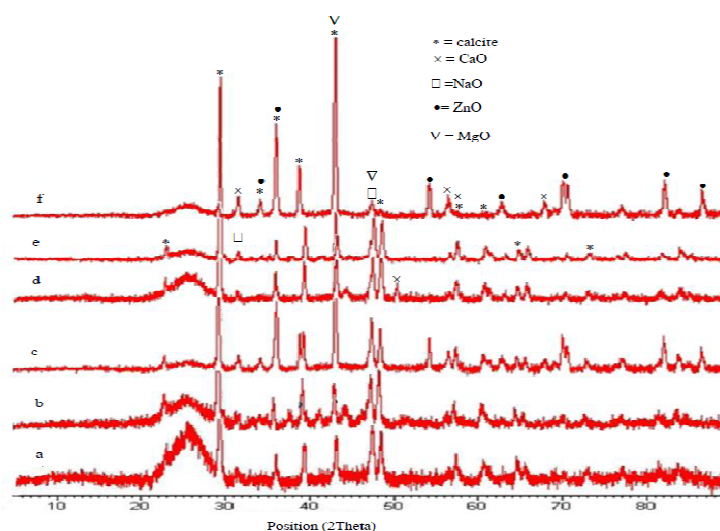
Fig. 2. FTIR transmittance spectra of (a) CHESM prepared at 400°C, (b) CHESM prepared at 500°C, (c) CHESM prepared at 600°C, (d) CH₃COONa-HESMAC prepared at 400°C, (e) CH₃COONa-HESMAC prepared at 500°C, (f) CH₃COONa- HESMAC prepared at 600°C, (g) Zn-HESMAC prepared at 400°C, (h) Zn-HESMAC prepared at 500°C and (i) Zn- HESMAC prepared at 600°C

Fig. 3. XRD patterns of (a) CDESM, (b) CH₃COONa-DESMAC, (c) Zn-DESMAC, (d) CHESM, (e) CH₃COONa-HESMAC and (f) Zn-HESMAC prepared at 600°C

The XRD peaks at 31.5, 40.5, 50.2, 54 and 57.5° are attributed to CaO (Mohammadi *et al*., 2014), which was formed from $CaCO_3$ by thermal degradation. XRD peaks of NaO, which formed from CH_3COONa by thermal degradation, are located at 32.1 and 47.4° (Magdziarz *et al*., 2016). The peaks present at 43, 49 and 75° are attributed to MgO, which originated from oxidation of Mg compounds found in the starting ESMs. Finally, the XRD diffraction peaks belonging to ZnO, which originated from oxidation of the Zn metal powder in Zn-DESMAC (Fig. 3c) and Zn-HESMAC (Fig. 3f), are located at 2θ = 31.7, 34.4, 36.2, 47.5, 56.6, 62.8, 66.3, 67.9 and 69.1° (Kashinath *et al*., 2016). The intensities of XRD peaks of Na_2O and ZnO in the activated products are higher after CH_3COONa and Zn addition in comparison to

products prepared without CH_3COONa and Zn additives carbonized. These XRD results correspond to FTIR and EDS data presented in Fig. 1 and 2 and Table 2.

SEM Analysis

The SEM images of the fresh DESM, CDESMs, CH_3COONa-DESMACs and Zn-DESMACs are shown in Fig. 4. The fresh DESM (Fig. 4a) shows a hierarchically ordered macroporous network and some microporous structures on the surface. After carbonization, the CDESMs show a network like structure with an aggregation of particles on the surface (Fig. 4b-d). The surfaces of CDESMs are quite smooth. The amount and size of particles on the surfaces of CDESMs decrease as the carbonization temperature is increased.
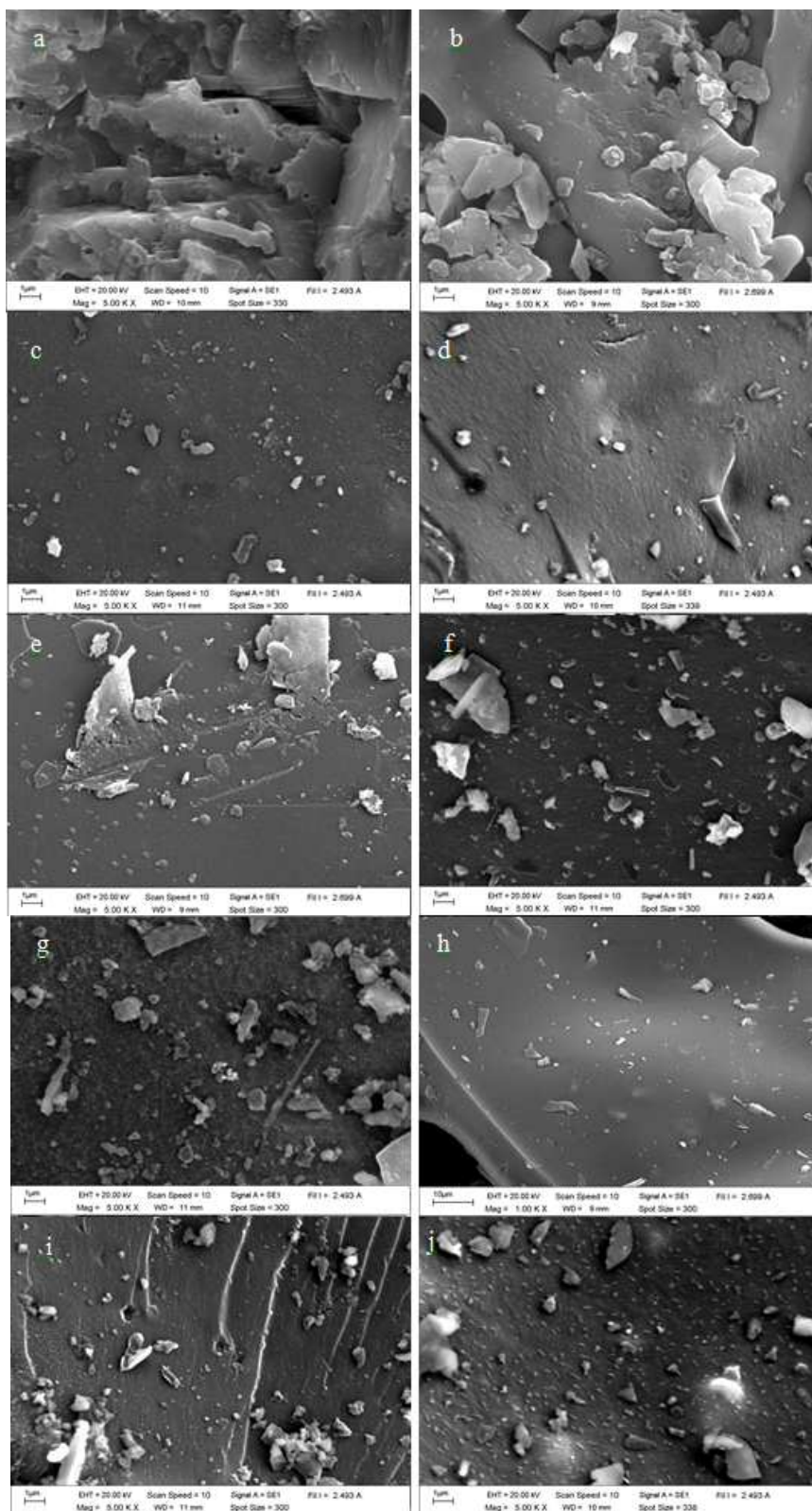
Fig. 4. Morphologies of (a) fresh DESM, (b) CDESM prepared at 400°C, (c) CDESM prepared at 500°C, (d) CDESM prepared at 600°C, (e) CH₃COONa-DESMAC prepared at 400°C, (f) CH₃COONa-DESMAC prepared at 500°C, (g) CH₃COONa-DESMAC prepared at 600°C, (h) Zn-DESMAC prepared at 400°C, (i) Zn-DESMAC prepared at 500°C and (j) Zn-DESMAC prepared at 600°C

The size of particles on the surface of CDESMs is 0.27-3.73, 0.09-1.18 and 0.05-1 μm for materials prepared at 400, 500 and 600 °C, respectively. This shows that the volatile compounds in DESM undergo a more extensive thermal degradation as higher carbonization temperatures. The activated products exhibit a more extensive thermal degradation than the CDESMs at same temperature (Fig. 4e-j). The CH_3COONa-DESMACs (Fig. 4e-g) show more open, porous and rough surfaces with spherical particles for activation at 500-600°C. The spherical particles with a diameter of about 90.9 nm are due to sodium oxide. However, the surface of CH_3COONa-DESMAC obtained with activation at 400°C does not show open porous structures. This indicates that the CH_3COONa-DESMAC prepared with activation at 400°C show small extent of degradation and partial oxidation. Furthermore, it was seen that the spherical particles on the surfaces CH_3COONa-DESMAC are firmly attached. This might be due to the fact that CH_3COONa can incorporate with proteins present in the ESMs fibers (Camaratta *et al.*, 2015). The amount of spherical particles and particles with uncertain shape increases as the activation temperature is increased, with especially high content at 600°C. This is because of volatile matters being degraded while Na_2O, CaO and some other metal oxides dominate the surface. Likewise, Zn-DESMACs (Fig. 4h-j) show high thermal degradation in comparison to CDESMs prepared at the same temperature. This result is related to the percent yield data in Table 1. At the activation temperature of 400°C, the smooth and quite clear surface containing only some particles is observed for Zn-DESMAC. However, Zn-DESMACs prepared at 500-600°C show surfaces with higher amounts of particles of various sizes in comparison to the material prepared at 400°C. It can be seen that the particles on Zn-DESMACs surface are attached more weakly than those on the surface of CH_3COONa-DESMACs prepared at the same temperature. This is attributed to low solubility of Zn metal in the reaction mixtures (Simanjuntak *et al.*, 2011). After activation at 600°C the Zn-DESMAC surface contains a high number of small particles that are regularly dispersed. Some large size particles can also be found on its surface (Fig. 4j).

Figure 5 shows the morphology of structures of the fresh HESM, CHESM, CH_3COONa-HESMAC and Zn-HESMAC. The morphology of fresh HESM (Fig. 5a) shows smooth interwoven fibers with some knobs and no porous structures on its surface. This is because the eggshell membrane mainly consists of fibrous or collagen like proteins (Tsai *et al.*, 2006). The diameter size of fresh HESM fiber is in the range of 1.71 to 4.86 μm. After carbonization at 400°C (Fig.

5b), CHESM shows smooth surface with some particles (0.23-10 μm diameter) and macroporous cavities (0.45-7.73 μm diameter). This shows that the volatile compounds, which coat the fibers, were thermally decomposed during the carbonization process. At this stage only the membrane matrix remained. After that, the rough characteristics with some differences in particle size (0.09-4.86 μm diameter) on the CHESM surface were observed after activation at 500°C (Fig. 5c). However, CHESM prepared at 600°C shows high amount of microporous structures with a small amount of differently sized particles (0.09-0.82 μm diameter) on the surface. After activation with CH_3COONa, the materials show that particles with differing sizes (0.05-4.82 μm) and shapes have accumulated on CH_3COONa-HESMAC at 400°C (Fig. 5e) to a greater extent than to which they formed on the surfaces of CHESMs. As the activation temperature is increased (from 500 to 600°C) a substantial amount of regularly dispersed small sized particles are formed on the surface of the HESMACs (Fig. 5f-g). A small amount of large particles also form on these products. It has been seen that the particles on HESMAC prepared at 600°C (Fig. 5f) became spherical in shape and larger in size (214.9-574.1 nm) in comparison to HESMAC prepared at 500°C (90.9-272 nm in diameter size) (Fig. 5g). However, quite clear and smooth surface with some rough character and particles was observed for Zn-HESMAC prepared at 400°C. Similarly, the high amount of differently sized particles (0.05-1.91 μm) were formed on Zn-HESMAC surface for the material prepared at 500°C (Fig. 5i). Furthermore, the high amount of spherical particles (about 45 nm diameter) with some large particles (0.182-2.091 μm diameter) was also observed on Zn-HESMAC surface for the material prepared at 600°C (Fig. 5j). These results indicated that Na_2O and ZnO accumulated on the surface of HESMACs after activation.

TEM Analysis

The TEM images shown in Fig. 6a and e reveal that the CDESM and CHESM prepared at 500°C consist of an amorphous carbon matrix. For material prepared with activation by CH_3COONa (at 500-600°C) and Zn (at 500°C), the TEM images of the activated products show some disordered graphite carbon matrix (Fig. 6b-d and f). Furthermore, it was seen that CH_3COONa-HESMAC prepared at 600°C (Fig. 6g) and Zn-HESMAC prepared at 500°C (Fig. 6h) show an amorphous carbon matrix with spherical particles (diameter of 68-578 nm) and nanofiber (diameter range of 13.51-43.24 nm), respectively. These results are consistent with XRD and SEM results.
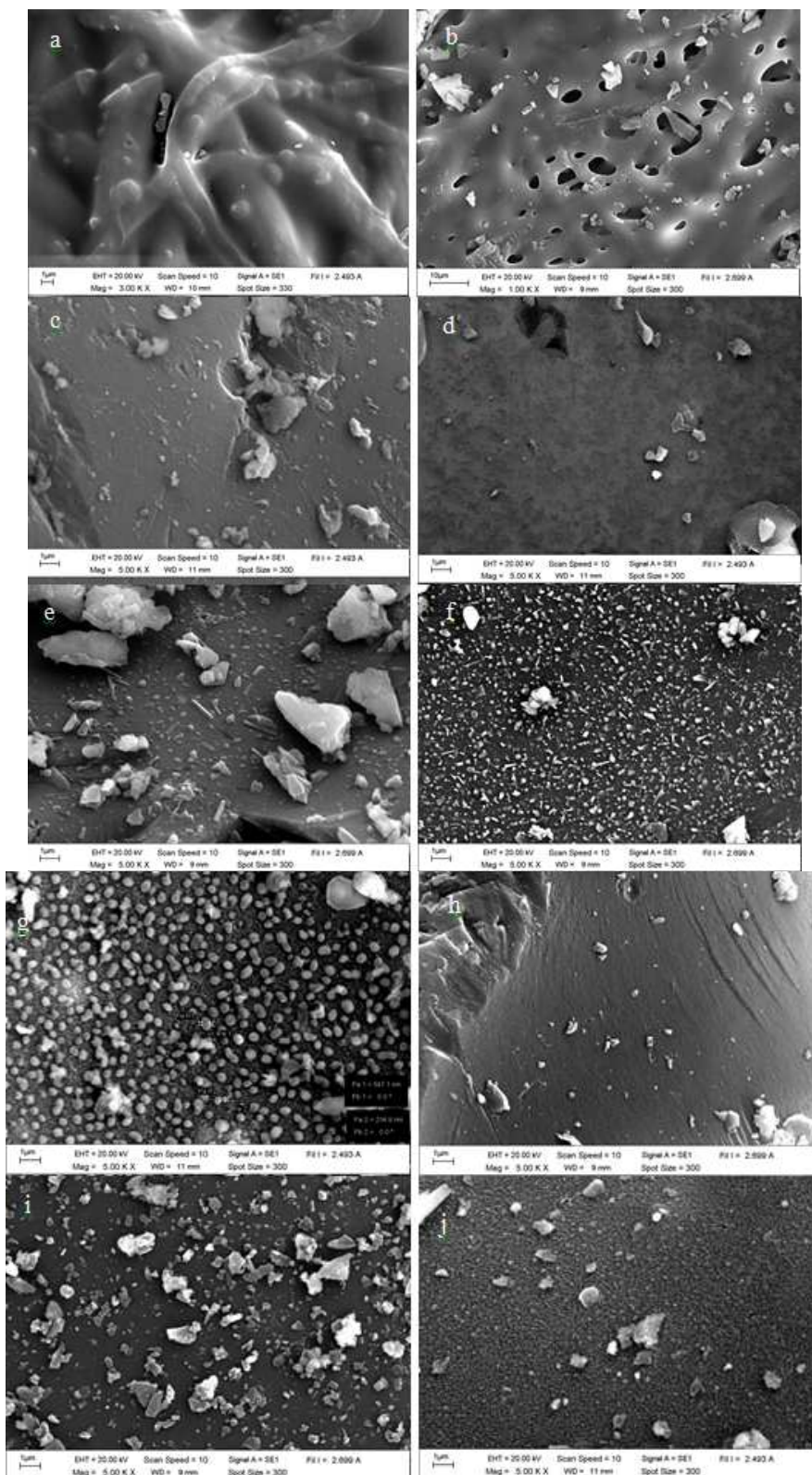
Fig. 5. Morphologies of (a) fresh HESM, (b) CHESM prepared at 400°C, (c) CHESM prepared at 500°C, (d) CHESM prepared at 600°C, (e) CH₃COONa-HESMAC prepared at 400°C, (f) CH₃COONa-HESMAC prepared at 500°C, (g) CH₃COONa-HESMAC prepared at 600°C, (h) Zn-HESMAC prepared at 400°C, (i) Zn-HESMAC prepared at 500°C and (j) Zn-HESMAC prepared at 600°C
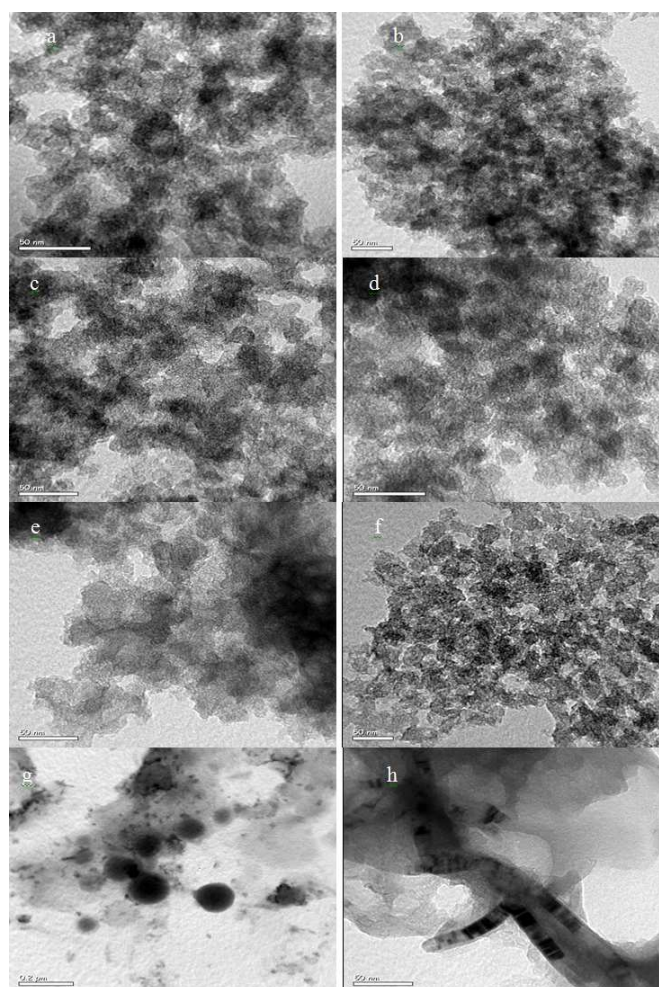
Fig. 6. TEM of (a) CDESM prepared at 500°C, (b) CH₃COONa-DESMAC prepared at 500°C, (c) CH₃COONa-DESMAC prepared at 600°C, (d) Zn-DESMAC prepared at 500°C, (e) CHESM prepared at 500°C, (f) CH₃COONa-HESMAC prepared at 500°C, (g) CH₃COONa-HESMAC prepared at 600°C and (h) Zn-HESMAC prepared at 500°C

Conclusion

It was concluded, based on the experimental results, that the percent yields of all carbonized and activated products have decreased with increasing carbonization or activation temperature. The results also show that all products prepared from DESM have percent yields higher than products prepared from HESM at the same conditions. There was a small relative decrease in the yield between 400 and 500°C followed by a high yield decrease between 500 and 600°C. The percent yields of ESMACs prepared using mixing with Zn metal were higher than those prepared using mixing with CH₃COONa at same temperature. The results have shown that some organic functionalities such as amines, amides, CO_3^{2-}, = C-H and = CH₂ groups still remain in CDESM after preparation at 400°C. It was shown that carboxylate of $CaCO_3$ is still incompletely decomposed after treatment at all activation temperatures. The C=C,

Na-O and C-O functional groups were also observed in ESMACs. Furthermore, it was shown that the CH₃COONa and Zn activation modes have no effect on the type of functional groups formed on the activated carbon products from both DESM and HESM. However, the additives have accelerated the decomposition or modification of functional groups on the surfaces of ESMACs. EDS analysis has shown that the HESMAC materials are mainly composed of carbon for both activation reagents and that their carbon content is higher than of the corresponding DESMACs. In addition, all activated carbon materials have quite high oxygen content, which is exhibited in high content of oxygen containing functional groups and metals oxide compound on the surfaces of the activated carbon materials. The XRD and TEM results of carbonized and activated products made from DESM and HESM displayed disordered graphite carbon structures and amorphous carbon. XRD patterns of ESMACs also showed crystalline calcite, CaO, MgO, ZnO

and Na$_2$O. The TEM images of CH$_3$COONa-HESMAC prepared at 600°C and Zn-HESMAC prepared at 500°C also show spherical particles (68-578 nm diameter) and nanofibers (13.51-43.24 nm diameter). The SEM morphologies of CDESMs are quite smooth but containing some particles. The amount and size of particles on the surfaces of CDESMs decrease as the carbonization temperature is increased. After activation at 500-600°C, ESMACs showed more open, porous and rough surface with spherical particles of sodium oxide or ZnO. It was seen that the particles on Zn-DESMACs are less firmly attached on the surface than those on CH$_3$COONa-DESMACs formed at the same activation temperature. Finally, it was also shown that the activation activity of CH$_3$COONa is stronger than that of Zn metal for ESMACs preparation. The characteristics of ESMACs observed in this study show that ESMACs can be considered for use as adsorbents for the removal the pollutants from water and other applications to achieve low-cost and also reduction of costs for waste disposal.

Acknowledgement

Funding Information

Author's Contributions

Sumrit Mopoung: Designed the research plan, organized the study and wrote of all paragraphs.

Kanjana Jitchaijaroenkul: Co-researchers who have reported and analyzed data presented in this paper.

Ethics

This article is original and contains unpublished material. The corresponding author confirms that all of the other authors have read and approved the manuscript and no ethical issues are involved.

References

Ahmed, T.A.E., H.P. Suso and M.T. Hincke, 2017. In-depth comparative analysis of the chicken eggshell membrane proteome. J. Proteomics, 155: 49-62.

Ayanda, O.S., O.S. Fatoki, F.A. Adekola and B.J. Ximba, 2013. Kinetics and equilibrium models for the sorption of tributyltin to nZnO, activated carbon and nZnO/activated carbon composite in artificial seawater. Mar. Pollut. Bull., 72: 222-230.

Baláž, M., 2014. Eggshell membrane biomaterial as a platform for applications in materials science. Acta Biomater., 10: 3827-3843.

Baláž, M., J. Ficeriová and J. Briančin, 2016. Influence of milling on the adsorption ability of eggshell waste. Chemosphere, 146: 458-471.

Botomé, M.L., P. Poletto, J. Junges, D. Perondi and A. Dettmer *et al.*, 2017. Preparation and characterization of a metal-rich activated carbon from CCA-treated wood for CO$_2$ capture. Chem. Eng. J., 321: 614-621.

Camaratta, R., J.O. Messana and C.P. Bergmann, 2015. Synthesis of ZnO through biomimetization of eggshell membranes using different precursors and its characterization. Ceram. Int., 41: 14826-14833. DOI: 10.1016/j.ceramint.2015.08.005

Gun'ko, V.M., V.M. Bogatyrov, O.I. Oranska, I.V. Urubkov and R. Leboda *et al.*, 2014. Synthesis and characterization of resorcinol-formaldehyde resin chars doped by zinc oxide. Applied Surf. Sci., 303: 263-271. DOI: 10.1016/j.apsusc.2014.02.164

Guo, X., F. Zhang, Q. Peng, S. Xu and X. Lei *et al.*, 2011. Layered double hydroxide/eggshell membrane: An inorganic biocomposite membrane as an efficient adsorbent for Cr(VI) removal. Chem. Eng. J., 166: 81-87.

Guru, P.S. and S. Dash, 2014. Sorption on eggshell waste—A review on ultrastructure, biomineralization and other applications. Adv. Colloid Interfac., 209: 49-67.

Kashinath, L., K. Namratha and K. Byrappa, 2016. Microwave assisted synthesis and characterization of nanostructure zinc oxide-graphene oxide and photo degradation of Brilliant Blue. Mater. Today Proc., 3: 74-83.

Kaewmanee, T., S. Benjakul and W. Visessanguan, 2009. Changes in chemical composition, physical properties and microstructure of duck egg as influenced by salting. Food Chem., 112: 560-569.

López Granados, M., M.D.Z. Poves, D.M. Alonso, R. Mariscal and F.C. Galisteo *et al.*, 2007. Biodiesel from sunflower oil by using activated calcium oxide. Applied Catal. B-Environ., 73: 317-326.

Magdziarz, A., A.K. Dalai and J.A. Koziński, 2016. Chemical composition, character and reactivity of renewable fuel ashes. Fuel, 176: 135-145.

Mami, M., A. Lucas-Girot, H. Oudadesse, R. Dorbez-Sridi and F. Mezahi *et al.*, 2008. Investigation of the surface reactivity of a sol–gel derived glass in the ternary system SiO$_2$-CaO-P$_2$O$_5$. Applied Surf. Sci., 254: 7386-7393.

Mittal, A., M. Teotia, R.K. Soni and J. Mittal, 2016. Applications of egg shell and egg shell membrane as adsorbents: A review. J. Mol. Liq., 223: 376-387. DOI: 10.1016/j.molliq.2016.08.065

Mohammadi, M., P. Lahijani and A.R. Mohamed, 2014. Refractory dopant-incorporated CaO from waste eggshell as sustainable sorbent for CO_2 capture: Experimental and kinetic studies. Chem. Eng. J., 243: 455-464. DOI: 10.1016/j.cej.2014.01.018

Mugisidi, D., A. Ranaldo, J.W. Soedarsono and M. Hikam, 2007. Modification of activated carbon using sodium acetate and its regeneration using sodium hydroxide for the adsorption of copper from aqueous solution. Carbon, 45: 1081-1084.

Myint, M.T.Z., S.H. Al-Harthi and J. Dutta, 2014. Brackish water desalination by capacitive deionization using zinc oxide micro/nanostructures grafted on activated carbon cloth electrodes. Desalination, 344: 236-242.

Nasrollahzadeh, M., S.M. Sajadi and A. Hatamifard, 2016. Waste chicken eggshell as a natural valuable resource and environmentally benign support for biosynthesis of catalytically active Cu/eggshell, Fe_3O_4/eggshell and Cu/Fe_3O_4/eggshell nanocomposites. Applied Catal. B Environ., 191: 209-227.

Pant, B., M. Park, H.Y. Kim and S.J. Park, 2017. CdS-TiO_2 NPs decorated carbonized eggshell membrane for effective removal of organic pollutants: A novel strategy to use a waste material for environmental remediation. J. Alloy. Compd., 699: 73-78.

Park, S., K.S. Choi, D. Lee, D. Kim and K.T. Lim *et al.*, 2016. Eggshell membrane: Review and impact on engineering. Biosys. Eng., 151: 446-463.

Rath, M.K., B.H. Choi, M.J. Ji and K.T. Lee, 2014. Eggshell membrane-templated synthesis of hierarchically-ordered NiO-$Ce_{0.8}Gd_{0.2}O_{1.9}$ composite powders and their electrochemical performances as SOFC anodes. Ceram. Int., 40: 3295-3304.

Simanjuntak, F.S.H., T.K. Kim, S.D. Lee, B.S. Ahn and H.S. Kim *et al.*, 2011. CaO-catalyzed synthesis of glycerol carbonate from glycerol and dimethyl carbonate: Isolation and characterization of an active Ca species. Applied Catal. A Gen., 401: 220-225. DOI: 10.1016/j.apcata.2011.05.024

Slimani, R., I.E. Ouahabi, F. Abidi, M.E. Haddad and A. Regti *et al.*, 2014. Calcined eggshells as a new biosorbent to remove basic dye from aqueous solutions: Thermodynamics, kinetics, isotherms and error analysis. J. Taiwan Inst. Chem. E., 45: 1578-1587. DOI: 10.1016/j.jtice.2013.10.009

Tan, Y.H., M.O. Abdullah, C. Nolasco-Hipolito and Y.H. Taufiq-Yap, 2015. Waste ostrich- and chicken-eggshells as heterogeneous base catalyst for biodiesel production from used cooking oil: Catalyst characterization and biodiesel yield performance. Applied Energ., 160: 58-70.

Tembe, S., B.S. Kubal, M. Karve and S.F. D'Souza, 2008. Glutaraldehyde activated eggshell membrane for immobilization of tyrosinase from *Amorphophallus companulatus*: Application in construction of electrochemical biosensor for dopamine. Anal. Chim. Acta, 612: 212-217.

Tong, H., P. Wan, W. Ma, G. Zhong and L. Cao *et al.*, 2008. Yolk sperocrystal: The structure, composition and liquid crystal template. J. Struct. Biol., 136: 1-9.

Tsai, W.T., J.M. Yang, C.W. Lai, Y.H. Cheng and C.C. Lin *et al.*, 2006. Characterization and adsorption properties of eggshells and eggshell membrane. Bioresource Technol., 97: 488-493.

Tsai, W.T., K.J. Hsien, H.C. Hsu, C.M. Lin and K.Y. Lin *et al.*, 2008. Utilization of ground eggshell waste as an adsorbent for the removal of dyes from aqueous solution. Bioresource Technol., 99: 1623-1629.

Yu, H., Q. Tang, J. Wu, Y. Lin and L. Fan *et al.*, 2012. Using eggshell membrane as a separator in supercapacitor. J. Power Sources, 206: 463-468. DOI: 10.1016/j.jpowsour.2012.01.116

Zaki, M.I., H. Knözinger, B. Tesche and G.A.H. Mekhemer, 2006. Influence of phosphonation and phosphation on surface acid–base and morphological properties of CaO as investigated by in situ FTIR spectroscopy and electron microscopy. J. Colloid Interf. Sci., 303: 9-17.